Surface Segregation and Formation of Silver Nanoparticles Created In situ in Poly(methyl Methacrylate) Films

Ranjan D. Deshmukh and Russell J. Composto*

Department of Materials Science and Engineering and Laboratory for Research on the Structure of Matter, University of Pennsylvania, Pennsylvania 19104-6272

Received August 28, 2006. Revised Manuscript Received December 8, 2006

Nanocomposite films have been prepared by the thermal decomposition of (1,1,1,5,5,5-hexafluoroacetylacetonato)silver(I) (AgHFA) in PMMA films containing 5, 10, and 20 wt % silver nanoparticles (NPs). When Rutherford backscattering spectrometry is used, as-cast films display a relatively uniform distribution of precursor in the midregion and a small excess of Ag near the surface, Z_s^*. Upon annealing at 185 °C, strong segregation of NPs to the surface and substrate is observed. The Z_s^* normalized by initial film thickness increases linearly with wt % Ag. For as-cast films, transmission electron microscopy (TEM) analysis shows that AgHFA forms small spherical domains (1−5 nm) prior to thermal decomposition. Upon preannealing at 107 °C, some aggregation of precursor is observed at the surface and substrate, consistent with the incompatibility of AgHFA with PMMA. Upon annealing at 185 °C, diffusion of the precursor to the surface and substrate occurs concurrently with NP formation. For 20 wt % Ag films, the NP diameters are 20−75 nm at the surface, 6 nm in the midregion, and 2−20 nm at the substrate. NP size and size distribution increase as the wt % Ag and annealing time increase. NPs near the surface are wet by a 1−5 nm thick polymer layer. Consistent with characterization studies, UV−visible spectroscopy shows a plasmon resonance attributed to Ag NPs. A model of the thermodynamic stability of submerged NPs is given and compared with experimental results. By understanding and controlling surface segregation and NP assembly, we can precisely control the surface conductivity and reflectivity in metal nanocomposite films.

Introduction

Nanocomposite polymeric films combine the attractive functional properties of nanoparticles (NPs) with the advantages of polymers, such as low cost. For example, by dispersing noble metal NPs in a matrix, we can utilize the third-order, nonlinear optical susceptibility of the NPs to prepare optical devices.[1] Nanocomposite films containing Ag NPs have potential as surface conductive polymeric tapes[2] and metal contacts for VLSI circuits. These films are also candidates for integral capacitors because they are easy to process at low temperature and exhibit a high dielectric constant.[3] The electrical,[4] mechanical,[5] catalytic,[6,7] and antibacterial properties[8] are also enhanced by adding NPs to polymers. In addition to NP size, shape, and concentration, film properties will depend on the NP−polymer interaction, which influences NP morphology (e.g., discrete versus aggregates). Whereas most studies have investigated preformed NPs added to polymers,[9] this study focuses on the surface and bulk composition, as well as the morphology, of nanocomposite polymeric films prepared by the in situ formation of NP within the polymer host.

Polymer nanocomposites can be prepared by several in situ methods. Gamma and ultraviolet irradiation have been used to prepare NPs of Ag in poly(vinyl alcohol),[10] PbS in poly(vinyl acetate),[11] CdS in poly(acryl amide),[12] Au in poly(acryl amide),[13] and Ag in poly(acrylonitrile).[14] Ion implantation, sputtering, vapor-phase co-deposition, and vacuum co-condensation have been used to prepare NPs of Ag in poly(methyl methacrylate)(PMMA),[15,16] Ag in silica,[17] Ag in Teflon,[18] and Pd, Sn, and Cu in poly(*p*-xylene).[19] NPs have also been formed by reducing metal salts in various

* To whom correspondence should be addressed. Telephone: 215-898-4451. Fax: 215-573-2128. Email: composto@seas.upenn.edu.

(1) Heilweil, E. J.; Hochstrasser, R. M. *J. Chem. Phys.* **1985**, *82*, 4762.
(2) Endrey, A. L. Electrically Conductive Polymeric Compositions. U.S. Patent 3 073 784, 1963.
(3) Pothukuchi, S.; Li, Y.; Wong, C. P. *J. Appl. Polym. Sci.* **2004**, *93*, 1531.
(4) Heilmann, A.; Kiesow, A.; Gruner, M.; Kreibig, U. *Thin Solid Films* **1999**, *344*, 175.
(5) Taylor, L. T. *Recent Advances in Polyimide Science and Technology*; Mid-Hudson Chapter of SPE: New York, 1987.
(6) Lewis, L. N. *Chem. Rev.* **1993**, *93*, 2693.
(7) Bond, G. C. *Surf. Sci.* **1985**, *156*, 966.
(8) Kim, J. W.; Lee, J. E.; Kim, S. J.; Lee, J. S.; Ryu, J. H.; Kim, J.; Han, S. H.; Chang, I. S.; Suh, K. D. *Polymer* **2004**, *45*, 4741.
(9) Bockstaller, M. R.; Mickiewicz, R. A.; Thomas, E. L. *Adv. Mater.* **2005**, *17*, 1331.
(10) Temgire, M. K.; Joshi, S. S. *Radiat. Phys. Chem.* **2004**, *71*, 1039.
(11) Qiao, Z. P.; Xie, Y.; Zhu, Y. G.; Qian, Y. T. *Mater. Sci. Eng., B* **2000**, *77*, 144.
(12) Qiao, Z. P.; Xie, Y.; Li, G.; Zhu,Y. J.; Qian, Y. T. *J. Mater. Sci.* **2000**, *35*, 285.
(13) Ni, Y. H.; Ge, X. W.; Zhang, Z. C.; Ye, Q. *Mater. Lett.* **2002**, *55*, 171.
(14) Zhang, Z. P.; Zhang, L. D.; Wang, S. X.; Chen, W.; Lei, Y. *Polymer* **2001**, *42*, 8315.
(15) Stepanov, A. L.; Popok, V. N.; Khaibullin, R. I.; Kreibig, U. *Nucl. Instr. Methods Phys. Res., Sect. B* **2002**, *191*, 473.
(16) Stepanov, A. L.; Khaibullin, R. I. *Rev. Adv. Mater. Sci.* **2004**, *7*, 108.
(17) Sarov, Y.; Nikolaeva, M.; Sendova-Vassileva, M.; Malinovska, D.; Pivin, J. C. *Vacuum* **2003**, *69*, 321.
(18) Biswas, A.; Aktas, O. C.; Kanzow, J.; Saeed, U.; Strunskus, T.; Zaporojtchenko, V.; Faupel, F. *Mater. Lett.* **2004**, *58*, 1530.
(19) Zavyalov, S. A.; Pivkina, A. N.; Schoonman, J. *Solid State Ionics* **2002**, *147*, 415.

10.1021/cm062030s CCC: $37.00
Published on Web 01/23/2007

types of polymers, including epoxy,[20] block copolymer,[21] and dendrimer.[22] A 1963 study showed that poly(amic acid) films containing a silver(I) carboxylate complex exhibit electrical conductivity upon curing.[2] This finding spurred investigations of various silver(I) salts, including nitrates and sulfates in poly(amic acid).[5,23,24] In the mid-1990s, Taylor and coworkers discovered that β-diketonate organometallic precursors form NPs in polyimide (PI) after curing.[25,26] Examples of these complexes include (1,1,1,5,5,5-hexafluoroacetylacetonato)(X)silver(I), AgHFA(X), where X is an alkene,[27] phosphine,[28,29] trans-bis(dimethylsilyl)ethene, bis(dimethyl)-ethylsilylacetylene, or allyltrimethylsilane.[30] In particular, AgHFA(1,5-cyclooctadiene), AgHFA(COD),[25,26] is an attractive complex because it is soluble in dimethylacetamide, DMAc, is a good solvent for poly(amic acid), forms a uniform near-surface layer of NPs in PI films, and produces reflective and conducting films. Thompson et al.[31−35] investigated a simpler β-diketonate (i.e., without stabilizing ligand, such as COD), namely AgHFA, which resulted in discrete NPs near the surface and highly reflective PI.

This paper will explore the surface and bulk morphology of poly(methyl methacrylate) (PMMA) nanocomposite films containing Ag NPs prepared by the thermal decomposition of AgHFA. PMMA is an attractive matrix for model studies because it is stable during NP formation, in contrast to poly(amic acid), which transforms to PI during curing. Although D'Urso et al.[36] observed the formation of Ag NPs (5−50 nm) in PMMA, the Ag concentration in the film decreased significantly (>90%) and rehomogenized during thermal treatment of AgHFA−PMMA at 200 °C. By contrast, the Ag concentration and NP distribution was stable in Ag−PI films prepared from AgHFA.[31−35] In Ag−PI, the surface-rich layer of Ag NPs is attributed to metal-promoted oxidative degradation of PI, which exposes Ag located at the surface to the environment. By contrast, the thermal stability of PMMA improves upon adding 0.5 wt % Ag NPs.[37] Thus, PMMA is a model matrix for studying how Ag concentration and annealing conditions influence NP formation, distribution, and segregation.

We herein report on the processing and characterization of Ag−PMMA films containing Ag NPs formed by thermal decomposition of the precursor AgHFA at 185 °C for 30−4320 min. The main result of this study is the strong segregation of Ag NPs to the surface and substrate. The surface excess of Ag normalized by film thickness increases linearly as the wt % Ag increases from 5 to 20 wt %. In this paper, we show evidence that upon annealing at 185 °C, the precursor diffuses to the surface and substrate because of its incompatibility with PMMA resulting, in excess precursor at the both interfaces. Concurrently, the NPs form by thermal decomposition of precursor and are enriched at the surface and substrate. For 20 wt % Ag films, the NP diameters are 20−75 nm at the surface, 6 nm in the midregion, and 2−20 nm at the substrate. For 5, 10, and 20 wt % Ag, the Ag concentration at the surface becomes nearly constant after 30 min of annealing at 185 °C. A thin polymer layer is found to wet NPs adjacent to the surface. Models created on the basis of the thermodynamics of an embedded particle and interparticle interactions are used to predict the stability of NPs near the surface. This paper brings together a range of characterization techniques and models that aim to improve our understanding and control over the formation, growth, and segregation of NPs in polymer films. Key properties such as surface conductivity and reflectivity can be tailored by precisely controlling the near surface morphology in metallic nanocomposites.[25,34,35]

Experimental Procedures

Materials. To prepare polymer nanocomposite films, we used silver acetate (CH_3COOAg), 1,1,1,5,5,5-hexafluoroacetylacetone (HFA), and methyl-isobutylketone (MIBK) from Sigma Aldrich without further purification. The poly(methyl methacrylate) (PMMA, M_w = 82.4K, PDI = 1.07) was acquired from Polymer Sources.

Methods. Whereas silver acetate is not soluble in MIBK, the organometallic complex AgHFA prepared from HFA and silver acetate is soluble in MIBK. To ensure complete complexation of silver acetate, we added HFA in slight excess (~10% by volume). PMMA powder was then added to this solution (4 mL) to make a solution of 9 wt % PMMA in MIBK. Assuming complete removal of the residual complex ($-OCCF_3-CH-CCF_3-O-$) during thermal decomposition, we varied the stoichiometry to produce PMMA films with 5, 10, and 20 wt % Ag. Thus, the wt % reported in this paper corresponds to the Ag NPs in the PMMA films after thermal decomposition. The AgHFA, PMMA, and MIBK solution was placed in 20 mL glass vials and mixed vigorously with a magnetic stirrer until a clear solution was observed, ~10 h. Because AgHFA is light sensitive, vials were wrapped in aluminum foil. The solution was poured through a Teflon filter with a pore size of 0.25 μm to remove impurities. This solution was spin-coated at 2000 rpm on precleaned and UV-treated (10 min) silicon and glass substrates to produce films from 500 to 700 nm thick. The films were preannealed in vacuum at 107 °C, which is slightly above the glass transition of PMMA (T_g = 105 °C), for 24 h to remove residual solvent. To induce NP formation, we then annealed films at 185 °C in Argon for 30−4320 min (3 days). For thermal gravimetric analysis, the precursor AgHFA was prepared by

(20) Zhi, L. J.; Zhao, T.; Yu, Y. Z. *Scr. Mater.* **2002**, *47*, 875.
(21) Abes, J. I.; Cohen, R. E.; Ross, C. A. *Mater. Sci. Eng., C* **2003**, *23*, 641.
(22) Balogh, L.; Tomalia, D. A. *J. Am. Chem. Soc.* **1998**, *120*, 7355.
(23) Auerbach, A. *J. Electrochem. Soc.* **1984**, *131*, 937.
(24) St. Clair, A. K.; Taylor, L. T. *J. Appl. Polym. Sci.* **1983**, *28*, 2393.
(25) Rubira, A. F.; Rancourt, J. D.; Caplan, M. L.; St. Clair, A. K.; Taylor, L. T. *Chem. Mater.* **1994**, *6*, 2351.
(26) Rubira, A. F.; Rancourt, J. D.; Taylor, L. T.; Stoakley, D. M.; St. Clair, A. K. *J. Macromol. Sci., Pure Appl. Chem.* **1998**, *A35*, 621.
(27) Doyle, G.; Eriksen, K. A.; Vanengen, D. *Organometallics* **1985**, *4*, 830.
(28) Lin, W. B.; Warren, T. H.; Nuzzo, R. G.; Girolami, G. S. *J. Am. Chem. Soc.* **1993**, *115*, 11644.
(29) Dryden, N. H.; Vittal, J. J.; Puddephatt, R. J. *Chem. Mater.* **1993**, *5*, 765.
(30) Itsuki, A.; Uchida, H.; Satou, M.; Ogi, K. *Nucl. Instr. Methods Phys. Res., Sect. B* **1997**, *121*, 116.
(31) Southward, R. E.; Thompson, D. S.; Thompson, D. W.; Caplan, M. L.; St. Clair, A. K. *Chem. Mater.* **1995**, *7*, 2171.
(32) Southward, R. E.; Thompson, D. S.; Thompson, D. W.; St. Clair, A. K. *Chem. Mater.* **1999**, *11*, 501.
(33) Southward, R. E.; Thompson, D. W. *Adv. Mater.* **1999**, *11*, 1043.
(34) Southward, R. E.; Thompson, D. W. *Mater. Des.* **2001**, *22*, 565.
(35) Southward, R. E.; Thompson, D. W. *Chem. Mater.* **2004**, *16*, 1277.
(36) D'Urso, L.; Nicolosi, V.; Compagnini, G.; Puglisi, O. *Mater. Sci. Eng., C* **2003**, *23*, 307.
(37) Zeng, R.; Rong, M. Z.; Zhang, M. Q.; Liang, H. C.; Zeng, H. M. *J. Mater. Sci. Lett.* **2001**, *20*, 1473.

dissolving silver acetate in HFA and MIBK. The solvent was evaporated in a vacuum at room temperature and the resulting solid, ~2 mg, was analyzed by TGA.

Characterization. Samples were characterized by a palette of techniques to evaluate thermal decomposition, the NP depth profile, and the NP characteristics beneath and at the surface. Thermal gravimetric analysis (TGA, TA Instruments, 4100 Thermal Analyzer) was performed at 5 °C/min as well as isothermally, 185 °C. Rutherford backscattering spectrometry (RBS, NEC Corporation 5 SDH Pelletron) was used to depth-profile silver in the nanocomposite film. RBS is particularly suited for depth-profiling heavy elements like Ag in a matrix of light elements.[38,39] For this study, a 2 MeV $^4He^+$ ion beam was incident at 10° with respect to the sample surface. To minimize radiation damage of PMMA, we kept the total charge low, 4 μC, and accumulated it in 0.5 μC increments on fresh areas. RUMP software was used to simulate RBS spectra and convert energy to depth. By fitting experimental spectra with simulations, we found the full width half-maximum (fwhm) depth resolution to be 55 nm. Simulations were performed by dividing the film into 3−6 sublayers of different atomic compositions and thickness values. The number of atoms per unit volume, or atomic density, is $N = \rho N_A N_o/M_o$, where ρ is mass density, N_A is Avogadro's number, N_o is number of atoms per monomeric unit, and M_o is molecular weight of the monomeric unit. For each sublayer, the volume fractions of Ag (V_{Ag}) and PMMA (V_{PMMA}) are chosen and $N_{Ag-PMMA}$ is calculated from $N_{Ag}V_{Ag} + N_{PMMA}V_{PMMA}$, where $N_{Ag} = 5.85 \times 10^{22}$ and $N_{PMMA} = 1.075 \times 10^{23}$ atoms/cm^3, respectively. The bulk densities of PMMA and Ag are 1.19 and 10.5 g/cm^3, respectively. By adjusting the thickness and volume fractions of each sublayer, we compared the simulation to the experimental data until a good fit was achieved. This simulation was used to calculate the total film thickness as well as the Ag surface and substrate excesses defined as

$$Z^* = \int_0^\infty (\phi(z) - \phi_\infty)dz \quad (1)$$

where $\phi(z)$ and ϕ_∞ are the atomic compositions at depth **z** and far from the interface, respectively. The depth $z = 0$ denotes the air/polymer or polymer/substrate interface. The atomic composition of Ag is defined relative to the monomer stoichiometry, namely $(C_5H_8O_2)_1Ag_\phi$.

The shape and size distribution of NPs were determined by transmission electron microscopy (TEM, Phillips 2010). Images were taken at 80 kV to minimize electron beam reduction of the precursor as well as degradation of PMMA. The cross-sections (~50−70 nm) for TEM were prepared by ultra-microtomy (Richtheart Jung Ultramicrotome) on films spin-coated on polyetherimide (PEI) substrates. The PEI substrates are attractive because they are dimensionally stable at 185 °C and easily cut by a diamond knife. Atomic force microscopy (Multimode AFM, Digital Instruments) was used to characterize NPs near the sample surface. The tip spring constant, resonance frequency, and diameter were 40 N/m, ~300 kHz, and <10 nm, respectively. Scan areas of 100 nm × 100 nm and 2 μm × 2 μm were collected in tapping mode at scan speeds of 0.25−0.75 Hz. The diameter, number density, and area fraction of NPs were determined using the Nanoscope III (Digital Instruments) and SPIP (Image Metrology) software. The optical properties of the Ag−PMMA nanocomposite were studied by UV−visible spectroscopy (Perkin-Elmer, Lambda Bio 40).

(38) Feldman L.C.; Mayer J.M. *Fundamentals of Surface and Thin Film Analysis*; Prentice Hall: Upper Saddle River, NJ, 1986.
(39) Composto, R. J.; Walters, R. M.; Genzer, J. *Mater. Sci. Eng., R* **2002**, *38*, 107.

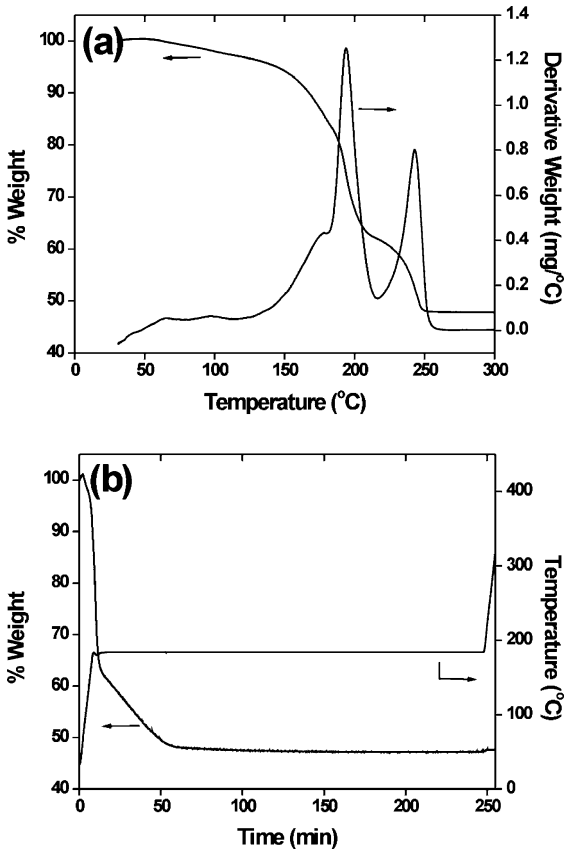

Figure 1. (a) Weight loss and derivative of weight loss of AgHFA precursor heated at 5 °C/min from 31 to 300 °C and (b) TGA of AgHFA upon rapid heating from 34 to 185 °C at 20 °C/min, followed by isothermal annealing at 185 °C for 4 h. To ensure complete conversion, we finally heated AgHFA from 185 to 300 °C at 20 °C/min.

Results

Thermal analysis of AgHFA was performed to determine the optimum temperature for the thermal decomposition of the AgHFA precursor in PMMA films. Figure 1a shows the weight loss and the derivative of weight loss of AgHFA between 31 and 300 °C at 5 °C/min. The first weight loss at 68 °C is attributed to the evolution of excess HFA (T_{bp} = 70 °C). The second loss near 110 °C results from the removal of acetic acid (T_{bp} = 118 °C) and trapped MIBK (T_{bp} = 116 °C). The thermal decomposition of the precursor occurs between 140 and 250 °C with a maximum rate of weight loss corresponding to derivative weight loss peaks near 194 and 242 °C. Whereas the ideal weight loss due to the evolution of the complexing agent is 65.7%, the measured weight loss is 52%. This lower measured weight loss value could be attributed to residual organic precursor. Isothermal TGA was performed to determine the time required for complete decomposition at 185 °C. Figure 1b shows a weight loss of 15% as the temperature increases at 20 °C/min from 34 to 185 °C over 7.55 min. After reaching isothermal conditions, the weight loss remains rapid up to 12 min before slowing down between 12 and 50 min. Consistent with the dynamic study in Figure 1a, the isothermal weight loss approaches a constant value of 52% after 60 min at 185 °C. To determine if complete decomposition was achieved, we subsequently heated the sample to 300 °C with no measurable weight loss, as shown in Figure 1b. Guided by these thermal analysis studies, we selected annealing conditions. Namely,

AgHFA−PMMA films were preannealed at 107 °C to remove residual solvent and then annealed at 185 °C to thermally decompose AgHFA and drive NP formation.

The depth profiles of silver in Ag−PMMA films were quantified by RBS. Figures 2a−c show backscattered counts as a function of depth for Ag−PMMA films containing 5, 10, and 20 wt % Ag. The counts are proportional to the atomic concentration of Ag in the film. For as-cast films (square symbols), the Ag concentration shows a small surface excess followed by a uniform distribution below ∼100 nm. As shown later, TEM is used to characterize the lateral distribution and morphology of Ag. After preannealing at 107 °C for 24 h (circles), the surface excess of Ag increases for films with 10 and 20 wt % Ag. The concentration of Ag remains relatively uniform across the middle of the film. After annealing for 30 min at 185 °C (triangles), the surface segregation of Ag strongly increases for all concentrations of Ag. Note that although the Ag counts are very small in the midregion,[40] TEM studies will reveal the existence of small NPs uniformly dispersed throughout the midregion of the film. For all samples at 185 °C, a small excess of Ag is observed at the polymer−silicon interface. This observation will also be supported by TEM studies. Films annealed for 30, 120 (downward triangle), and 4320 min (diamond) show similar depth profiles. As discussed later, annealing for 120 and 4320 min results in the coarsening of the NPs, which is consistent with the broadening of the surface layer shown in panels b and c of Figure 2. For films annealed at 185 °C, the integrated areas under the surface peaks are similar, indicating that Ag does not diffuse back into the film. Moreover, Ag is not lost after thermal treatment in contrast to prior studies.[36]

For each processing condition, the RBS spectra (e.g., Figure 2) were simulated to determine the concentration profile of Ag that has segregated to the surface and substrate. Figure 3a shows the surface excess (Z_s^*) as a function of processing condition. Although a small value, Z_s^* is measurable in the as-cast film, indicating that some segregation of AgHFA occurs during spin-casting. Upon preannealing, Z_s^* increases strongly as the wt % of Ag increases. After 30 min at 185 °C, Z_s^* increases to its maximum value for 10 and 20 wt % Ag and very close to its maximum for 5 wt %. Longer annealing times result in a small decrease in Z_s^* for films with 10 and 20 wt % Ag. As shown in Figure 2, Ag also segregates to the substrate, which, for example, corresponds to the 300−500 nm region in Figure 2a. For annealed films, interfacial segregation Z_i^* is much weaker than surface segregation and reaches values of only 4, 3, and 3 nm (± 1 nm) at 5, 10, and 20 wt % Ag, respectively. For the 5, 10, and 20 wt % Ag−PMMA films, the initial thickness, h_o, values are 513, 558, and 701 nm, respectively. Upon annealing at 185 °C, thickness values decrease to 500, 550, and 570 nm, respectively, independent of time. Because the RBS depth resolution is 55 nm, the decrease in thickness is readily observed only for films with the highest Ag concentration. Figure 3b shows that the normalized surface excess, Z_s^*/h_o, increases linearly as the wt % Ag increases. Thus, the surface concentration of Ag is found to scale with the bulk concentration added to the film.

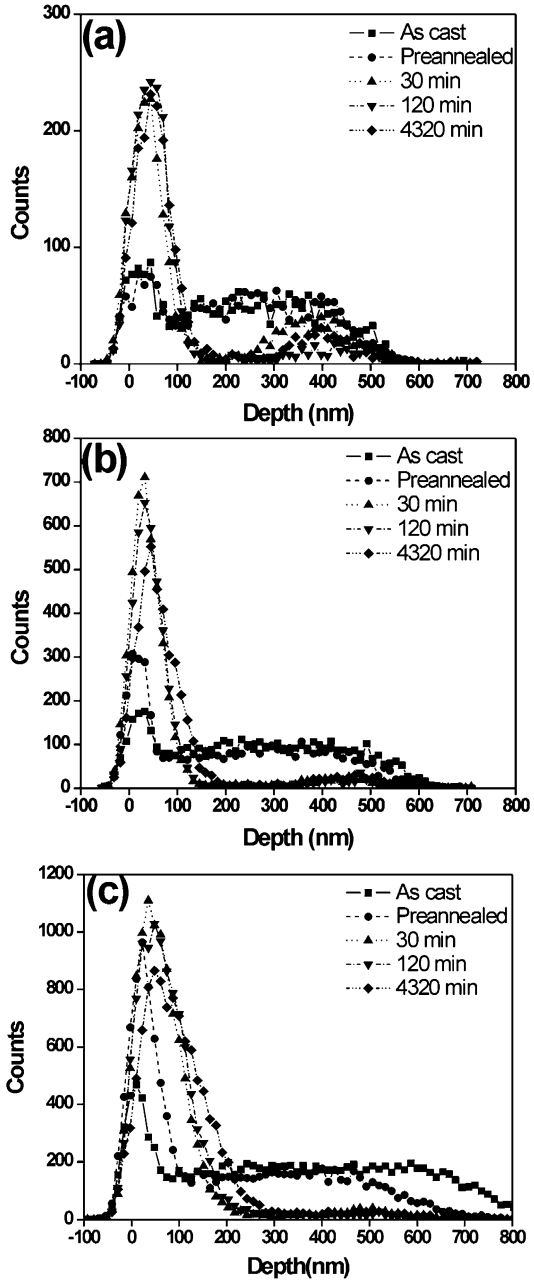

Figure 2. Rutherford backscattering (RBS) spectra for nanocomposite films containing (a) 5, (b) 10, and (c) 20 wt % Ag. Counts correspond to backscattering events from Ag. Films correspond to as-cast, preannealed to remove solvent and annealed at 185 °C to form nanoparticles. The as-cast films show uniform Ag distribution in the mid-region and a small surface excess of Ag. Preannealing increases the surface excess at 10 and 20 wt % Ag. Upon annealing, strong segregation to the surface and weak segregation to the substrate is observed at all concentrations. Although the surface peak broadens with time, the integrated area remains relatively fixed after 30 min.

Whereas RBS provides a quantitative analysis of the Ag depth profile, TEM and AFM provide the lateral imaging capabilities for following the morphology evolution of AgHFA−PMMA films. Figure 4 shows cross-sections of 20 wt % Ag films (a, b) as-cast, (c, d) preannealed, and (e, f) annealed for 120 min. The arrow identifies the film/PEI interface. Figure 4a shows that the AgHFA precursor is uniformly distributed in the film, and the slight segregation

(40) The substrate excess is only apparent in Figure 2a because the maximum on the *y*-axis is only 300 counts.

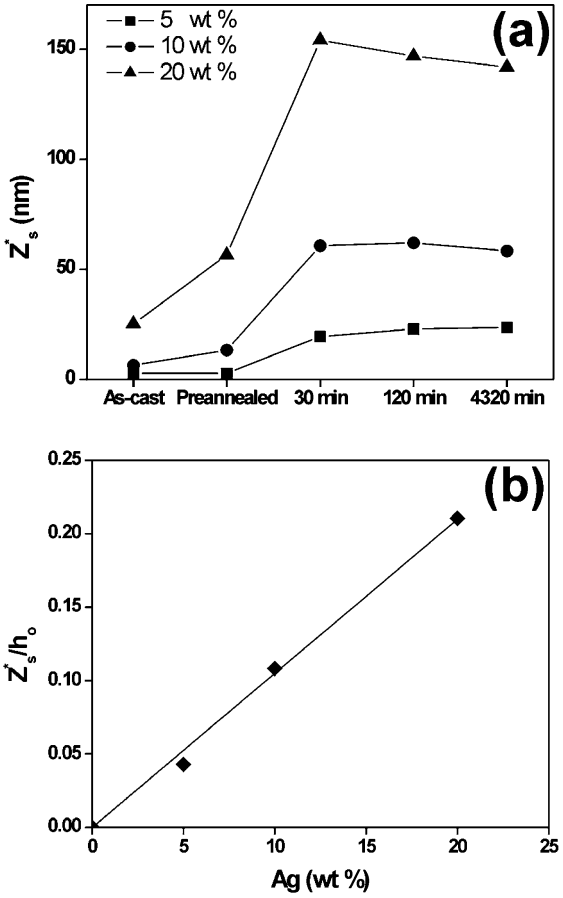

Figure 3. (a) Surface excess (Z_s^*) as a function of processing conditions for 5, 10, and 20 wt % Ag. (b) Surface excess normalized by the initial film thickness (Z_s^*/h_o) as a function of wt % of Ag. Here, Z_s^* is the average value determined at 30, 120, and 4320 min in (a). The solid line is a linear fit using $Z_s^*/h_o = 0.0105 \times$ (wt % Ag) and $R^2 = 0.99$.

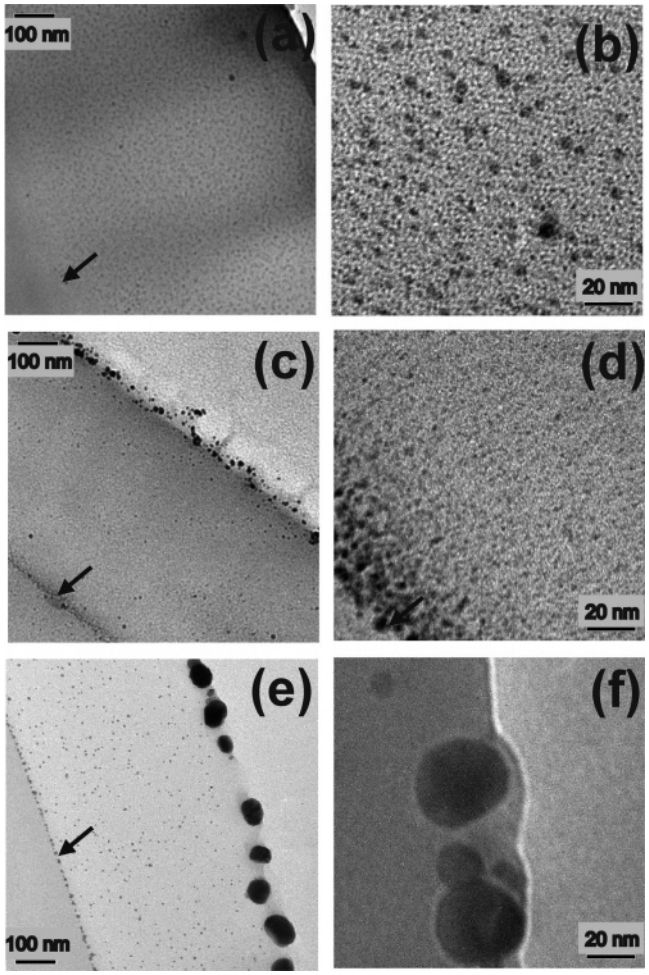

Figure 4. Transmission electron microscopy (TEM) cross-sectional images for films containing 20 wt % Ag (a, b) as-cast, (c, d) preannealed, and (e, f) annealed for 120 min at 185 °C. Arrows denote the polymer/PEI interface.

found by RBS is not observed. For the first time, AgHFA is observed to assemble into spherical domains from 1 to 5 nm (Figure 4b) prior to NP formation (i.e., thermal decomposition of AgHFA). Upon preannealing, Figure 4c shows that aggregates from 2 to 15 nm are located near the surface, consistent with the surface segregation of Ag observed in RBS specta shown in Figure 2. Figure 4d provides direct evidence that the aggregates segregate to the PEI substrate. After annealing, three populations of NPs are observed, namely those at the surface, substrate, and midregion, as shown in Figure 4e. The largest NPs form near the surface and exhibit diameters from 20 to 75 nm. By inspection of Figure 4e, we find that these NPs are responsible for a surface-rich Ag layer ~60 nm thick. The smallest NPs are uniformly dispersed across the midregion and have diameters of 5.7 ± 1.9 nm. The low density of NPs in the midregion is consistent with the low counts in the midregion of the RBS spectra (Figure 2). At the film/PEI interface (arrow), moderate (20 nm) to small (2 nm) NPs are observed, although at a much lower density than the surface. This observation is again consistent with RBS results. Unfortunately, TEM and RBS results cannot be quantitatively compared because each technique requires different substrates for characterization. However, TEM cross-sections on PEI and RBS spectra on silicon both show strong surface and weak substrate segregation of NPs. This agreement suggests that substrate type (i.e., silicon versus PEI) has a minor effect on surface segregation of NPs. However, because Ag is likely to interact differently with silicon oxide (on Si) and PEI, future studies are necessary to determine if the concentration and morphology in the near-substrate region is modified by substrate type.

TEM is an excellent technique for high-resolution imaging of individual NP. Figure 4f shows that NPs adjacent to the surface are covered by a polymer layer a few monomers thick (1−5 nm). The realization of an insulating layer between NPs and the surface, unreported in prior studies, is practically important because this layer will reduce the surface conductivity of metallized films. Figure 5 shows high-resolution TEM images of individual NPs located in the middle of an annealed film. Figure 5a shows (111) fringes with a 2.36 Å lattice spacing, consistent with the formation of crystalline Ag.[41] In addition, a few large NPs (>30 nm) near the surface exhibit crystalline facets as shown in Figure 5b. Electron diffraction patterns (Figure 5b, inset) further support the crystallization of the NPs.

AFM was used to characterize precursor aggregation and NP formation near the surface of as-cast and preannealed films. Figure 6 shows AFM images of the as-cast (left column) and preannealed (right column) films containing 5,

(41) Daly, C.; Krim, J. *Phys. Rev. Lett.* **1996**, *76*, 803.

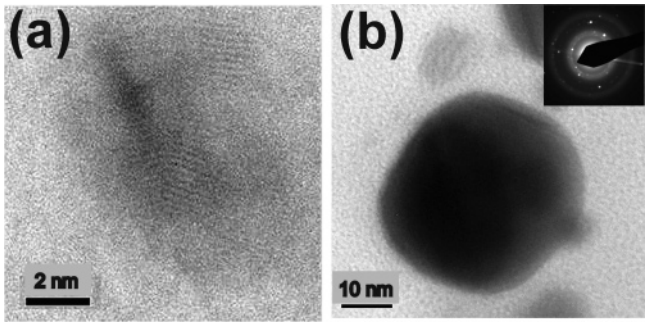

Figure 5. (a) High-resolution TEM image of a NP (~6 nm) from the midregion of a Ag−PMMA film showing (111) lattice fringes. (b) Faceted NP (~30 nm) located near the polymer surface. The inset shows the electron diffraction pattern from this NP.

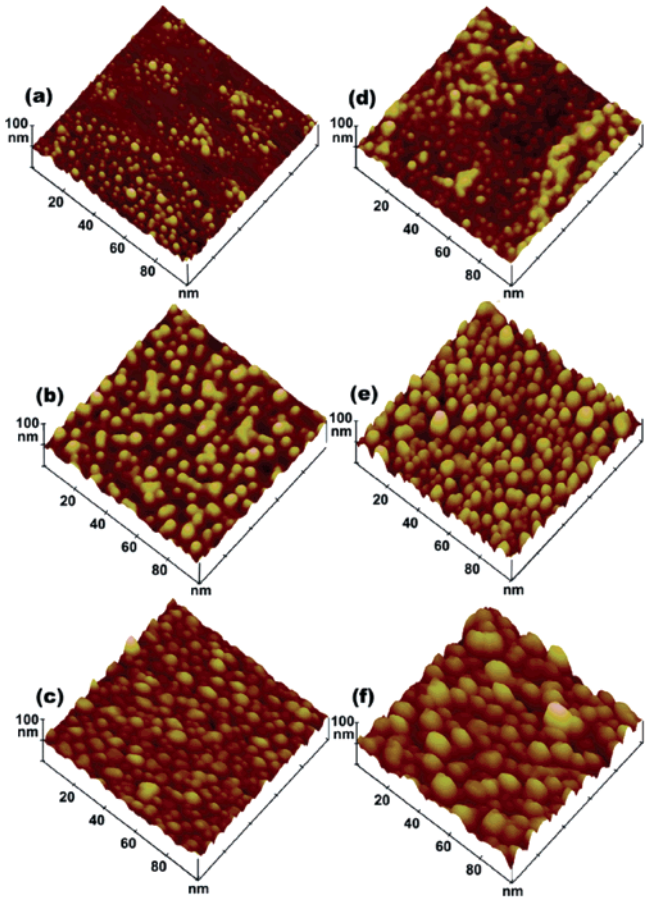

Figure 6. AFM images of as-cast films (left column) showing islandlike features for (a) 5, (b) 10, and (c) 20 wt % Ag. AFM images of preannealed films (right column) for (d) 5, (e) 10, and (f) 20 wt % Ag. The height scale is 100 nm. All images are plotted on a 100 nm × 100 nm scale.

10, and 20 wt % Ag (top to bottom). For the as-cast films, small, hemispherical features protrude out of the surface (i.e., islands). As shown in Figure 6a−c, the island diameter increases from 2 to 3.5 to 4.0 nm as the wt % Ag increases. Concurrently, the island density increases as the wt % Ag increases. After preannealing (Figure 6d−f), island size and density increase relative to the as-cast films at each wt %. This behavior is consistent with the segregation of Ag as observed by RBS (Figure 2) and TEM (Figure 4c).

AFM was also used to characterize the surface morphology of films annealed at 185 °C. Figure 7a−i shows the effect of annealing time on (a−c) 5, (d−f) 10, and (g−i) 20 wt % Ag−PMMA films. A histogram of the island size distribution is superimposed over each figure. Note that the diameter measured by AFM is larger than the real NP diameter measured by TEM (e.g., Figure 4e) because of the finite tip size and the PMMA wetting layer covering the NPs (Figure 4f). At each time, the island size and area fraction increase, and the number density decreases as the concentration of Ag increases from 5 to 20 wt %. At fixed Ag concentration, the island size increases and the number density and area fraction decrease as annealing time increases from 30 to 4320 min. Note that the island size distribution broadens as the Ag concentration increases. These trends in the island diameter, number density, and area fraction are quantified in Figure 8a−c, respectively, and are discussed in the next section.

Discussion

The specular reflectivity and surface conductivity of metallic nanocomposite films depend on the surface concentration of metal and the surface morphology of the NPs. Why the concentration of NPs at the surface surpasses the bulk value after thermal treatment is not yet understood. For as-cast films of AgHFA−PMMA, nanophase-separated, precursor-rich regions are observed (images a and b of Figure 4), suggesting that AgHFA is incompatible with PMMA. These precursor-rich regions are spherical (1−5 nm) and weakly attracted to the surface (Figures 2 and 6a−c) and distribute uniformly in the midregion of the film (Figure 4a). Upon preannealing, the surface excess of Ag increases for 10 and 20 wt % Ag relative to the as-cast films (Figure 3a). This increase in Z_s^* is attributed to the diffusion of the precursor to the surface. A main finding of this paper is that precursor diffusion prior to thermal treatment is partly responsible for the high density of NPs located near the surface. Direct evidence for precursor aggregation near the surface is given in Figure 4c. Precursor diffusion to the substrate as well as aggregation near the substrate is also observed as shown in Figure 4d. The driving force for diffusion to the surface and substrate is likely the incompatibility of AgHFA with PMMA.

In AgHFA−PMMA films, the reduction of Ag^{+1} can occur during preannealing. To ensure complete reduction of Ag^{+1} to Ag^0 as well as NP formation, we subsequently annealed films at 185 °C. However, some unneutralized Ag^+ can remain after thermal decomposition. Using X-ray photoelectron and Auger electron spectroscopies, Rubira et al.[25] have shown that silver ions in AgHFA-doped polyimide films may not be completely converted to silver metal. These Ag^+ ions are expected to be reduced by the polymer and either remain bound to PMMA or attach to a NP. Thus, we expect a low concentration of unneutralized Ag^+ in PMMA films although it is difficult to estimate the exact amount. This annealing induces the decomposition of organometallic precursors by loss of ligand, ligand dissociation, and the formation of reactive, unsaturated organometallic species.[42−44] The remaining unsaturated metal fragments or metallomers then

(42) Heck, R. F.; Breslow, D. S. *J. Am. Chem. Soc.* **1961**, *83*, 1097.
(43) Ungvary, F.; Marko, L. *J. Organometallic Chem.* **1969**, *20*, 205.
(44) Werner, H.; Ault, B. S.; Orchin, M. *J. Organometallic Chem.* **1978**, *162*, 189.

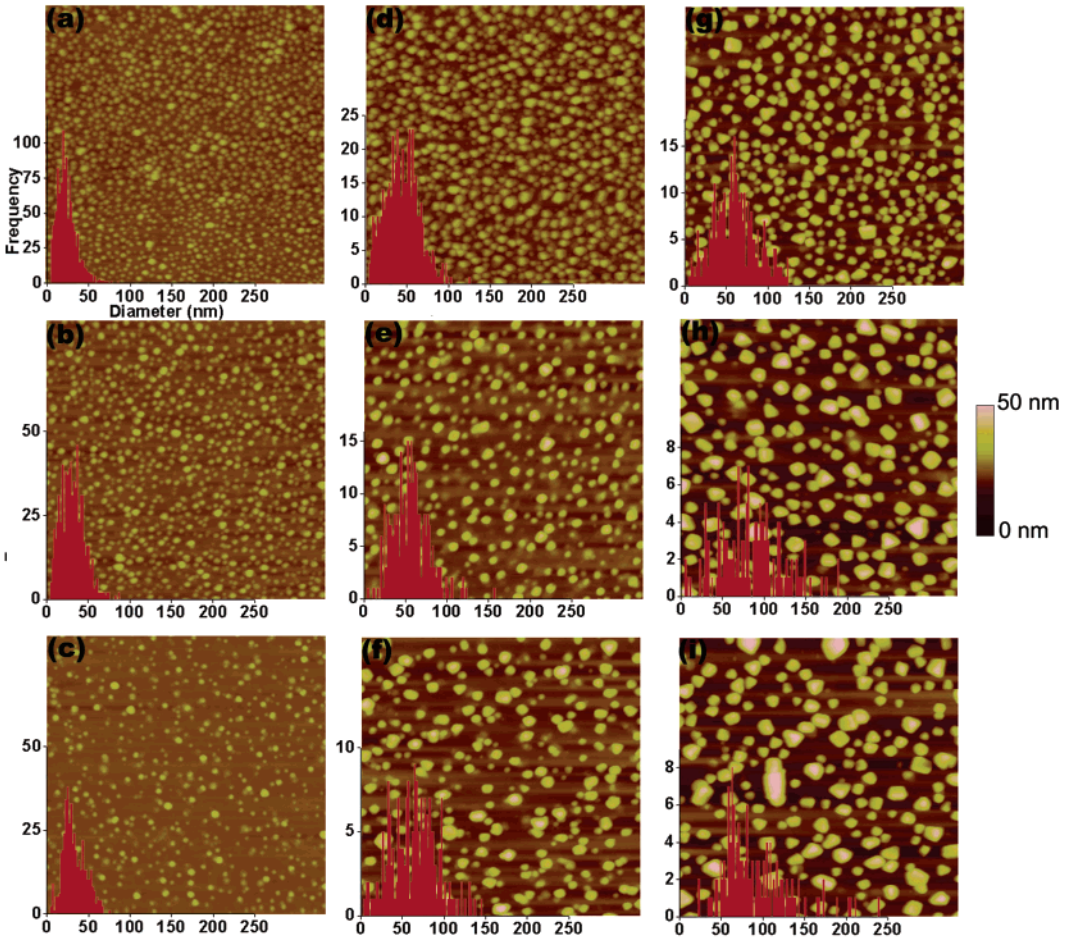

Figure 7. Nanoparticle size and size distribution (superimposed) determined by AFM as a function of annealing time (top to bottom) and wt % of Ag (left to right). Images of (a−c) 5, (d−f) 10, and (g−i) 20 wt % Ag−PMMA films. The films were annealed at 185 °C for (a, d, g) 30, (b, e, h) 120, (c, f, i) and 4320 min. All images are 2 μm × 2 μm. Frequency represents the number of particles at a particular diameter. Diameter corresponds to the size of the protruding NP covered by the PMMA wetting layer.

initiate the nucleation and growth of NPs.[45] Concurrent with thermal decomposition, the precursor or intermediate species diffuse to the polymer surface and substrate. As a result, the precursor concentration increases at both interfaces, which leads to the surface and substrate enrichment of NPs as observed in Figure 2. Because the precursor contains fluorine (i.e., CF_3), surface segregation may also be driven by the low surface energy of the complexing agent, namely HFA. For example, nanocomposites prepared by thermal decomposition of AgHFA(COD) in polyimide exhibit a fluorine-rich surface and interface.[25] To test this hypothesis in our study, we prepared nanocomposites of PMMA with a nonfluorinated precursor, silver nitrate, $AgNO_3$. For $AgNO_3$−PMMA films containing 5 wt % Ag, RBS studies show an enrichment of Ag at the surface, indicating that a F-rich complexing agent is not required to drive surface segregation. However, we have found that anion type influences the kinetics of surface enrichment; namely, segregation of Ag is much slower for the $AgNO_3$−PMMA films compared to the AgHFA−PMMA films at 5 wt % Ag. Detailed studies of $AgNO_3$−PMMA films are required for understanding the role of anion type on the kinetics of surface segregation.

PMMA chains can sterically stabilize precursor aggregates that form during casting and preannealing. We note that precursor aggregate formation indicates that the AgHFA complex has limited solubility in PMMA. However, after removal of HFA and formation of neutral NPs of Ag, a favorable interaction between the NP and PMMA promotes miscibility. Namely, Zeng et al.[37] showed that Ag has a favorable interaction with the O (mainly from the C═O group) in PMMA. In $AgNO_3$−poly(vinyl alcohol) mixtures, favorable interactions between Ag and O have also been reported.[46,47] Thus, once NPs have formed, the stabilization of Ag is enhanced by adsorbed PMMA chains. Overall, the formation of large NPs that appear at the surface is a complicated process that depends on miscibility of precursor with PMMA, thermal decomposition of precursor, NP formation, and the coarsening of aggregates/NPs that occur during annealing. Further studies are needed to evaluate the thermodynamic and dynamic contributions leading to the final morphology. The precursor concentration near interfaces can be increased by either the before mentioned diffusion process or increasing the bulk concentration. Upon annealing, the large precursor aggregates near the surface and substrate

(45) King, S.; Hyunh, K.; Tannenbaum, R. *J. Phys. Chem. B* **2003**, *107*, 12097.
(46) Zidan, H. M. *Polym. Test.* **1999**, *18*, 449.
(47) Yen, C. C.; Chang, T. C.; Kakinoki, H. *J. Appl. Polym. Sci.* **1990**, *40*, 53.

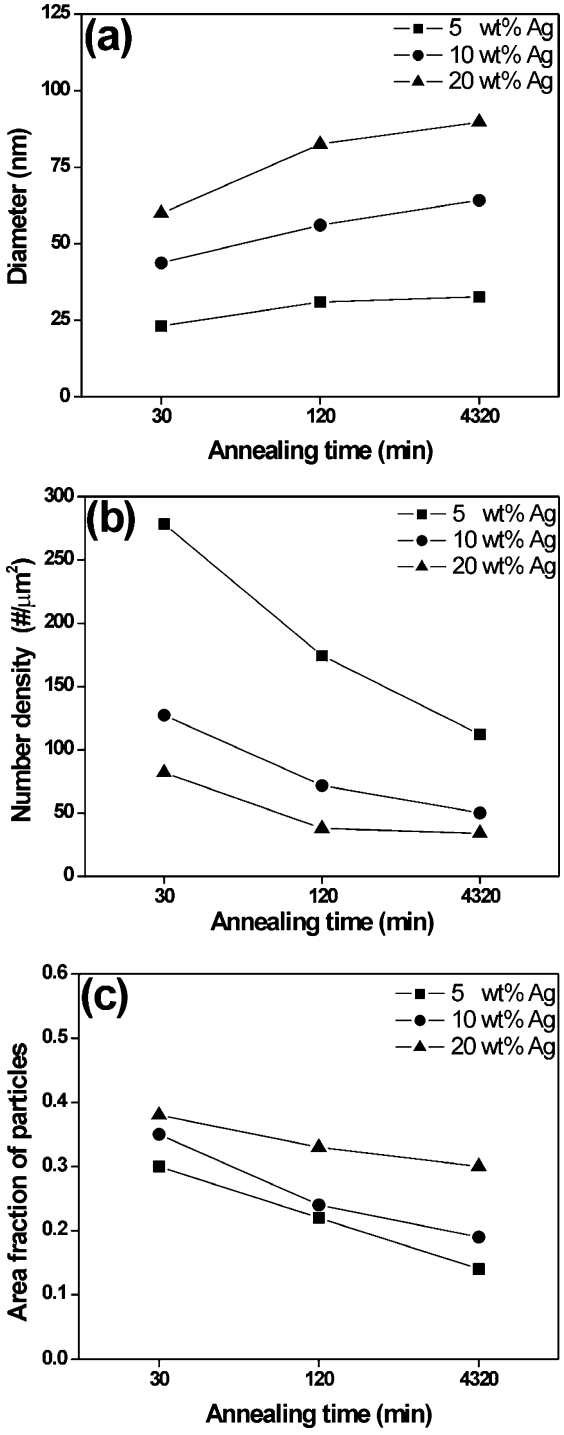

Figure 8. (a) Diameter, (b) number density, and (c) area fraction of NP as a function of annealing time at 185 °C. This data is taken from AFM images such as those shown in Figure 7.

transform into large NPs. This behavior explains why (a) NPs near the surface and substrate are larger than those in the midregion, at constant wt %, as shown in Figure 4e, and (b) the NP size increases on increasing the precursor concentration, as shown in Figure 8a.

Upon annealing at 185 °C, the Ag NP size increases and number density decreases with increasing annealing time, as shown in panels a and b of Figure 8, respectively. Moreover, the Ag surface peak broadens in the RBS spectra shown in Figure 2. These results suggest that NP growth can occur by a coarsening mechanism whereby large particles grow at the expense of smaller ones. Coarsening has been observed for Ag particles embedded in a glass matrix.[48] In this study, the growth kinetics of silver obeyed Oswald ripening where the particle diameter grew as $t^{1/3}$. This growth is diffusion controlled and its rate is determined by atomic diffusion and the reaction of Ag at the glass−particle interface.[48] In our study, the limited data in Figure 8a prevents a rigorous test of the Oswald mechanism.

The growth of NPs can also occur by particle coalescence. If neighboring particles approach, they can coalesce by diffusion of metal atoms along the particle surface even if the annealing temperature is below the bulk melting temperature, T_{mp}. For gold NPs (diameter = 5 nm) in polymer films, coalescence was estimated to occur very rapidly, 1×10^{-6} s, at 180 °C.[49] Because the present study uses much longer annealing times and a slightly higher temperature, coalescence of Ag NPs at 185 °C is worth consideration. Particles can melt and coalesce at relatively low temperatures because the melting point of NP is lower than T_{mp}.[50] The depression in the melting temperature is a direct consequence of the large internal stress acting on a particle due its surface.[51] For embedded particles, the magnitude of melting point depression depends on the surface energy (γ) and interfacial energy (γ_i).[51] The literature values for Ag NPs, which are free and embedded in different matrices, are γ = 6.4[52] and 7.2[53] J/m^2 and γ_i = 5.9−1.3 J/m,[2,52,54,55] respectively. For bulk Ag, γ = 1.065−1.54 J/m^2.[53] We have calculated the melting temperature of Ag NP embedded in a PMMA matrix as a function of NP size using the model by Castro et al.[51] For selected γ_i values of 3.5, 2.5, 1.4 J/m^2, Ag NPs with diameters of 8, 5.2, and 2.1 nm have a melting temperature of 185 °C. Upon annealing, the NPs at the surface that form directly from the precusor aggregates are greater than 10 nm and thus solid at 185 °C. Thus, melting point suppression is unlikely to contribute significantly to particle coarsening at the surface.

Catalytic degradation of the matrix has been used to explain Ag NP growth near the surface of PI films.[9] In these studies, a temperature of 300 °C was needed to complete the conversion of poly(amic acid) to PI. After annealing for 2−3 h, the growth of Ag NPs near the surface was attributed to the degradation of PI chains, which was catalyzed by small Ag NPs. Because of PI degradation near the surface, small metal particles were able to contact each and form larger NPs at the surface. The degradation of PI also exposes the NPs at the surface, presumably resulting in the observed conducting and reflective surface.[9] In contrast to the Ag−PI studies, Ag−PMMA nanocomposite has been reported to be thermally more stable than the PMMA matrix.[37] In our study,

(48) Yata, K.; Yamaguchi, T. *J. Mater. Sci.* **1992**, *27*, 101.
(49) Kay, E. *Z. Phys. D* **1986**, *3*, 251.
(50) Jiang, Q.; Zhang, S.; Zhao, M. *Mater. Chem. Phys.* **2003**, *82*, 225.
(51) Castro, T.; Reifenberger, R.; Choi, E.; Andres, R. P. *Phys. Rev. B* **1990**, *42*, 8548.
(52) Hofmeister, H.; Thiel, S.; Dubiel, M.; Schurig, E. *Appl. Phys. Lett.* **1997**, *70*, 1694.
(53) Nanda, K. K.; Maisels, A.; Kruis, F. E.; Fissan, H.; Stappert, S. *Phys. Rev. Lett.* **2003**, *91*, 106102.
(54) Montano, P. A.; Schulze, W.; Tesche, B.; Shenoy, G. K.; Morrison, T. I. *Phys. Rev. B* **1984**, *30*, 672.
(55) Dubiel, M.; Hofmeister, H.; Schurig, E. *Phys. Status Solidi B* **1997**, *203*, R5.

Ag−PMMA films were nonconducting because, even at 20 wt % Ag, the NPs were well-separated (cf., Figure 7). Furthermore, a thin 1−5 nm wetting layer of PMMA covers Ag NPs near the surface (cf., Figure 4f) resulting in a nonconducting surface. Taken together, these results suggest that PMMA is stable and that coarsening of Ag NPs in Ag−PMMA films is not attributed to the degradation of the matrix.

To reduce the surface free energy, a wetting layer of PMMA covers the Ag NPs, which has important consequences for surface properties. Although expected upon comparison of the surface energies of PMMA and Ag, direct evidence for this thin wetting layer in metallic nanocomposites has not been presented in previous studies. Thus, if NP happen to be exposed at the surface, a polymer wetting layer will spread over the NP and engulf the particle. Note that the wetting layer in Figure 4f is not flat but rather has a curvature that produces a pressure directed toward submerging the NP. Kovacs et al.[56] expressed the condition for complete sinking of an individual particle on a soft substrate as

$$\gamma_1 > \gamma_2 + \gamma_i \tag{2}$$

where γ_1 and γ_2 are the surface tensions of particle and the polymer and γ_i is the interfacial tension. If this condition is not met, NP can partially sink into the substrate. For Ag NPs, $\gamma_{Ag} = 6.4$ J/m^2 > $\gamma_{PMMA} + \gamma_{Ag-PMMA}$, where γ_{PMMA} is 0.028 J/m^2 at 185 °C[57] and $\gamma_{Ag-PMMA}$ is in the range 1.3−5.9 J/m^2. Thus, complete sinking is expected for Ag NPs in PMMA. This driving force may be responsible for the decrease in the area fraction of NPs and Z_s^* at long annealing times as shown in Figure 8c and Figure 3a, respectively. The sinking of the NPs may also explain the decrease in reflectivity observed in Ag−polyimide films at long times.[35]

Although surface energy arguments support NP sinking, Ag NPs appear stable near the surface even after annealing for 4320 min at 185 °C. In an attempt to understand this behavior, a thermodynamic model from Kovacs et al.,[58] is used to predict the equilibrium location of a sphere of radius a where the top of the sphere is located a distance z below the polymer surface. The free-energy change for a particle near the surface is $\Delta F = \Delta U_{VDW} - T\Delta S$. The van der Waals (dispersion) interaction is responsible for attracting the particle toward the bulk of the polymer (i.e., away from the surface) and is given by

$$\Delta U_{VDW} = \frac{A_{12}}{6}\left[\frac{2+2x}{2x+x^2} + \ln\left(\frac{x}{2+x}\right)\right] \tag{3}$$

where A_{12} is the Hamaker constant between Ag and PMMA and $x = z/a$. The polymer chains adjacent to the particle have lower entropy (fewer conformations) relative to a free chain. This entropic cost is reduced as the particle moves closer to the surface because chains adjacent to the particle can access more conformations at the surface. Thus, the entropic term drives the particle toward the surface. The change of entropy of polymer adjacent to a particle located at depth z relative to polymer near a particle far from the surface

$$\Delta S = k\frac{N_P N}{V}\cdot\frac{b^2}{6}4\pi a\epsilon\left[1 - \sinh\beta_o\sum_{n=0}^{\infty}\frac{\exp[-(n+{}^1/_2)\beta_o]}{\cosh[(n+{}^1/_2)\beta_o]}\right] \tag{4}$$

where $\beta_o = \sinh^{-1}\{[x(x+2)]^{0.5}\}$, k is the Boltzmann constant, N_P is the total number of polymer chains, N is the degree of polymerization, V is the volume occupied by polymer, b is the statistical length, and ϵ is a parameter related to the increase in polymer density adjacent to the particle. Results are relatively insensitive to the value of ϵ. Thus, as the particle moves far from the surface (i.e., large x), β_o approaches infinity, the bracketed term in eq 4 approaches 0, and ΔS goes to zero. However, as the particle approaches the surface, β_o approaches 0 and the bracketed term goes to a finite value, 1 − ln 2. As x varies from far below the surface to the surface, β_o varies monotonically,[58] and thus eq 4 captures the gain in chain entropy that originates from the conformational freedom near the surface (i.e., relaxation of chain compression adjacent to a particle). An alternative explanation for interpreting the increase in ΔS for chains near the surface is that free chains intersperse the region around the particle and increase the configurational entropy of adsorbed chains. Experimental studies using isotopic blends of PMMA would be required to test this hypothesis. The particle position is determined by balancing enthalpy gain (particle attraction) against entropy cost (chain conformation). In eq 3, $a = 25 \times 10^{-9}$ m (TEM) and $A_{12} = 16.67 \times 10^{-20}$ J. A_{12} is calculated from $A_{12} = \sqrt{A_{11}A_{22}}$,[59] using $A_{11} = 39.10 \times 10^{-20}$ J[60] and $A_{22} = 7.11 \times 10^{-20}$ J,[61] for Ag and PMMA, respectively. For eq 4, $b = 6.6 \times 10^{-10}$ m,[62] $N_P N/V$ was calculated to be 6.9×10^{27} m^{-3}, and $\epsilon = 0.03$.[58] Using these values, we find that the particle is at an equilibrium position for $z = 60$ nm. Figure 4f shows that the top of the Ag NPs are located at a depth of ∼1−5 nm, which is at least an order of magnitude closer to the surface than predicted by the model. The depth of the 1D potential well, $\Delta F_{minimum}$, is 2.76×10^{-21} J. Because the thermal fluctuation energy is $kT/2 = 3.16 \times 10^{-21}$ J, this model is unable to capture the observed stability of Ag NPs near the surface of Ag−PMMA films.

To improve upon this model, Kovacs et al.[58] suggested that interparticle interactions can stabilize a monolayer of particles in the near-surface region. The van der Waals binding energy was calculated assuming six symmetrical, equidistant, and equiplanar nearest neighbors for each particle. If the central particle is displaced a distance h below the plane, the interaction potential energy due to the six nearest neighbors is

$$E_{VDW} = -A_{121}\left[\frac{2a^2}{h^2 + R_o{}^2 - 4a^2} + \frac{2a^2}{h^2 + R_o{}^2} + \ln\left(\frac{h^2 + R_o{}^2 - 4a^2}{h^2 + R_o{}^2}\right)\right] \tag{6}$$

where R_o is the center-to-center distance between two

(56) Kovacs, G. J.; Vincett, P. S. *Thin Solid Films* **1984**, *111*, 65.
(57) Bandrup, J.; Immergut, E. H.; Grulke, E. A. *Polymer Handbook*, 4th ed.; Wiley-Interscience: New York, 1999.
(58) Kovacs, G. J.; Vincett, P. S. *J. Colloid Interface Sci.* **1982**, *90*, 335.

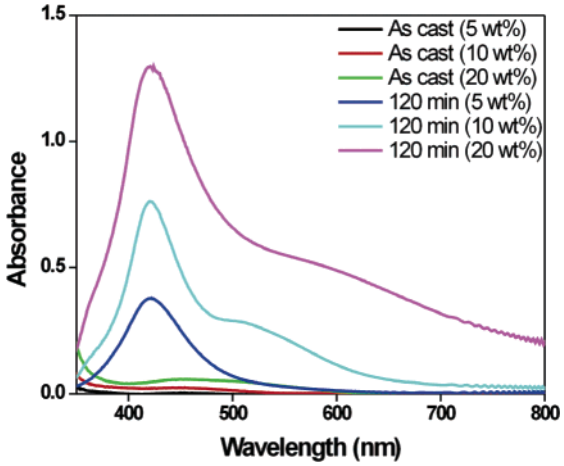

Figure 9. UV−visible spectroscopy for as-cast and annealed films containing 5, 10, and 20 wt % Ag. The as-cast films exhibit low absorbance. However, upon annealing at 185 °C for 120 min, a strong plasmon absorbance peak near 422 nm is observed because of the Ag NP. The peak absorbance increases, but does not shift position, as the Ag content increases from 5 to 20 wt %. However, a shoulder appears for the 10 and 20 wt % Ag.

neighbors, A_{121} is the Hamaker constant due to the interaction between two spheres embedded in the PMMA matrix. Assuming hexagonal packing, $R_o = 3a$, and using $A_{121} = (\sqrt{A_{11}} - \sqrt{A_{22}})^2 = 12.86 \times 10^{-20}$ J,[59] eq 6 gives $E_{VDW} = 4.43 \times 10^{-21}$ J. Although larger than the other model, this energy is also the same magnitude as the thermal fluctuation energy and thus may not be sufficient to stabilize the NPs near the surface. For a more rigorous test, the model should be modified to account for a distribution of particle size, particle−polymer interaction, and stronger interactions between particles. Nevertheless, this model provides a good starting point for understanding why NPs locate at the surface.

Optical Properties. The optical properties of Ag−PMMA films containing 5, 10, and 20 wt % Ag were measured by UV−visible spectroscopy, as shown in Figure 9. For all concentrations, as-cast films absorb very weakly over the UV−visible range. However, upon annealing for 120 min at 185 °C, films exhibit a plasmon absorption peak at 422 nm, which is consistent with the formation of nanometer metal particles. Plasmon resonance results from the collective oscillation of free electrons in NPs in response to an external electric field.[63] The resonance position and shape depends on the particle type, size, and shape as well as the dielectric constant of the matrix.[63] Although the peak position remains fixed, the plasmon peak broadens appreciably as the Ag concentration increases from 5 to 20 wt %. The peak intensity also increases as the Ag concentration increases and is strongest at 20 wt % Ag.

The size and shape of the NPs determines the characteristics of the plasmon resonance.[63−66] As the diameter of spherical particle increases, the plasmon resonance shifts toward longer wavelengths (i.e., red shift). However, the plasmon resonance peak can also shift to longer wavelengths if the NP shape changes from a sphere to cube (or pentagon or triangle).[66] The peak at 422 is consistent with spherical NPs (40−50 nm)[66] and is characterized by TEM. At 10 and 20 wt % Ag, the resonance peak broadens because the NP size distribution broadens, as shown in Figure 7. Although not observed at 5 wt % Ag, spectra for the 10 and 20 wt % films display a high wavelength shoulder in the resonance peak. This shoulder may correspond to plasmon absorption from faceted NPs (e.g., cubic, pentagon). For Ag−PMMA films at 10 and 20 wt % Ag, faceted NPs were observed by AFM (not shown) and high-resolution TEM (Figure 5b). Comparing absorbance at 422 nm to the shoulder, we find that the population of spherical NPs is much larger than that of the faceted NPs, which is consistent with experimental observations.

Conclusion

We have used complementary characterization techniques like RBS, TEM, and AFM to understand and control the formation, growth, and stratification of NPs in PMMA. In this study, Ag NPs were synthesized in situ in PMMA films by thermal decomposition of AgHFA. Although surface enrichment of Ag NPs was previously observed, the reason for segregation was not entirely clear. In this paper, we propose a mechanism for the segregation and formation of NP at the surface and substrate. Prior to thermal decomposition, precursor aggregates form because of the incompatibility of precursor with PMMA. Upon annealing at 185 °C, diffusion of the precursor to the surface and substrate occurs concurrently with NP formation, which results in NPs that are enriched at the surface and substrate relative to the midregion. Models created on the basis of thermodynamics of an embedded particle and interparticle interactions failed to account for the stability of the surface-segregated NPs. Therefore, a new model, which takes into account the polymer particle interaction and other factors mentioned in this paper, is required for explaining the stability of the NPs near the surface.

Acknowledgment. This work was supported by the National Science Foundation Polymer (DMR02-34903), MRSEC (DMR05-20020), NSEC (DMR04-25780) Programs. Acknowledgment is made to the donors of the American Chemical Society Petroleum Research Fund for partial support.

CM062030S

(59) Israelachvili, J. N. *Intermolecular and Surface Forces*; Academic Press: San Diego, 1991.
(60) Eichenlaub, S.; Chan, C.; Beaudoin, S. P. *J. Colloid Interface Sci.* **2002**, *248*, 389.
(61) Buscal, R.; Corner, T.; Stageman, J. F. *Polymer Colloids*; Elsevier Applied Science: New York, 1985.
(62) Fetters, L. J.; Lohse, D. J.; Richter, D.; Witten, T. A.; Zirkel, A. *Macromolecules* **1994**, *27*, 4639.
(63) Kreibig, U.; Vollmer, M. *Optical Properties of Metal Clusters*; Springer-Verlag: Berlin, 1995.
(64) Im, S. H.; Lee, Y. T.; Wiley, B.; Xia, Y. *Angew. Chem.* **2005**, *117*, 2192.
(65) Xia, Y.; Halas, N. J. *Mater. Res. Bull.* **2005**, *30*, 338.
(66) Mock, J. J.; Barbic, M.; Smith, D. R.; Schultz, D. A.; Schultz, S. *J. Chem. Phys.* **2002**, *116*, 6755.